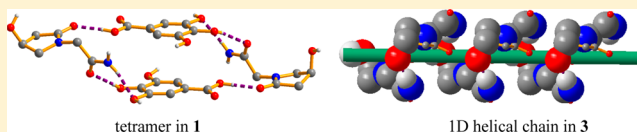


Enhancing the Hygroscopic Stability of *S*-Oxiracetam via Pharmaceutical CocrystalsZi-Zhou Wang,[†] Jia-Mei Chen,^{*,‡} and Tong-Bu Lu^{*,†,‡}[†]MOE Key Laboratory of Bioinorganic and Synthetic Chemistry, State Key Laboratory of Optoelectronic Materials and Technologies, School of Chemistry and Chemical Engineering, Sun Yat-Sen University, Guangzhou 510275, China[‡]School of Pharmaceutical Sciences, Sun Yat-Sen University, Guangzhou 510006, China

Supporting Information

ABSTRACT: Four cocrystals of (*S*-ox)(ga) (1), (*RS*-ox)(ga) (2), (*S*-ox)(pa) (3), and (*RS*-ox)(pa) (4) were prepared (*S*-ox = *S*-oxiracetam, *RS*-ox = racemic oxiracetam, ga = gallic acid, pa = 3,4-dihydroxybenzoic acid), and their structures were determined by single X-ray diffraction. In 1/2, two ga molecules link two *S*-ox/*RS*-ox molecules through intermolecular hydrogen bonds with a new $R_2^2(9)$ synthon to form a tetramer, the tetramers are further linked by intertetramer hydrogen bonds to generate a 2D sheet, and the adjacent 2D sheets are connected by intersheet hydrogen bonds to form the 3D structure of 1/2. In 3/4, the ox molecules form a 1D helical chain through intermolecular hydrogen bonds, and the helical chains are further linked by pa molecules through intermolecular hydrogen bonds to form a 2D sheet. The results of hygroscopic stability experiments indicate that the hygroscopic stability of *S*-ox is much enhanced after the formation of cocrystal 1.



INTRODUCTION

During the past decades, chiral drugs have been playing a significant role in the pharmaceutical industry. By the year of 2002, chiral drugs with a single enantiomer dosage form share 39% of the world market,¹ and the number is increasing year by year. According to the guidance of development of new chiral drugs,² single enantiomers of new drugs are encouraged to be developed, and a single enantiomer for a certain drug can be marketed under a different name to its racemic mixture.

The nootropic drug oxiracetam (4-hydroxy-2-oxo-1-pyrrolidine acetamide, ox) was first synthesized by Smith Kline Beecham Company in 1974.³ It is a racemic compound comprised of *S*-ox and *R*-ox (see Scheme 1). The structure of racemic oxiracetam (*RS*-ox) has been reported,⁴ while the structure of its single enantiomer (*S*-ox or *R*-ox) has not been reported so far. It has been reported that *S*-ox has better performance than *RS*-ox in treatment of cognition dysfunction.⁵ However, we found that *S*-ox is heavily hygroscopic and deliquesces to a liquid within 3 days at 87% RH and 25 °C, while *RS*-ox is stable under the same conditions, and this is in accordance with Wallach's rule,^{6–12} which states that a racemic crystal is expected to have a higher density than its chiral counterpart, resulting in a more efficient packing and higher overall stability.¹³ Recently, Jones et al.⁷ first found that the hygroscopic stabilities of chiral and racemic cocrystals also follow a trend of Wallach's rule: that is, the racemic cocrystal appears to be more stable than its chiral counterpart. However, their results are based only on two sets of cocrystals, and it needs more examples to confirm this assumption.

In order to enhance the hygroscopic stability of *S*-ox and to see whether the stability of their chiral and racemic cocrystals follows the Wallach's rule, four cocrystals of (*S*-ox)(ga), (*RS*-ox)(ga), (*S*-ox)(pa), and (*RS*-ox)(pa) were synthesized (ga = gallic acid, pa = 3,4-dihydroxybenzoic acid,¹⁴ see Scheme 1), and their structures and hygroscopic stability were investigated.

(*S*-ox)(ga), (*S*-ox)(pa), and (*RS*-ox)(pa) were synthesized (ga = gallic acid, pa = 3,4-dihydroxybenzoic acid,¹⁴ see Scheme 1), and their structures and hygroscopic stability were investigated.

EXPERIMENTAL SECTION

General Remarks. *S*-ox and *RS*-ox were provided by Sichuan Industrial Institute of Antibiotics. All of the cofomers were purchased from Aladdin Reagent Corporation. The solvents were commercially available and used without further purification. Elemental analyses were determined using an Elementar Vario EL elemental analyzer. The IR spectra were recorded in the 4000 to 400 cm⁻¹ region using KBr pellets and a Thermo Scientific AVATAR330 FT-IR spectrometer. Differential scanning calorimetry (DSC) was carried out on a Netzsch STA 409PC instrument in N₂ atmosphere. X-ray powder diffraction (XRPD) patterns were obtained on a Bruker D8 Advance with Cu K α radiation (40 kV, 40 mA).

(*S*-ox)(ga), 1. A mixture of *S*-ox (0.158 g, 1 mmol) and ga (0.170 g, 1 mmol) was dissolved in 3 mL of methanol in a sealed flask, and stirred at room temperature for 5 h. The resulting solution was filtrated and evaporated slowly at room temperature. After about one week, colorless prism-shaped crystals of 1 were isolated by filtration, washed with diethyl ether, and dried under vacuum. Yield: 0.30 g, 91%. Anal. Calcd for C₁₃H₁₆N₂O₈: C, 47.56; H, 4.91; N, 8.53. Found: C, 47.32; H, 5.12; N, 9.00%. IR data (KBr, cm⁻¹) 3754 vs, 3195 s, 2980 m, 2375 w, 1686 s, 1659 s, 1604 m, 1495 w, 1451 m, 1396 m, 1349 w, 1285 s, 1248 m, 1077 w, 939 m, 863 w, 763 w, 706 w, 612 m, 457 w.

(*RS*-ox)(ga), 2. A mixture of *RS*-ox (0.158 g, 1 mmol) and ga (0.170 g, 1 mmol) was stirred in 10 mL of ethanol in a sealed flask for 24 h, and the solution was filtrated and evaporated slowly at room temperature. After about 2 weeks, colorless prism-shaped crystals of 2

Received: June 2, 2012

Revised: July 24, 2012

Published: August 7, 2012

Scheme 1. Structures of Oxiracetam and Cofomers

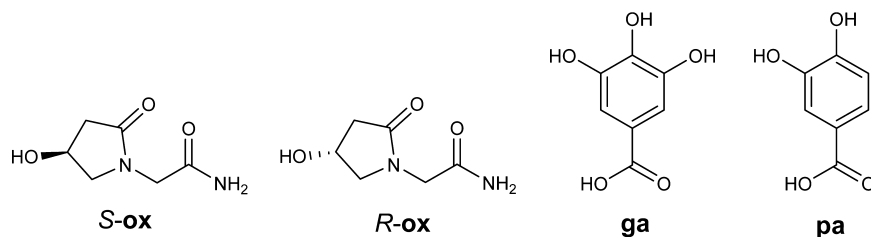


Table 1. Crystallographic Data and Details of Refinements for 1–4

	1	2	3	4
formula	C ₁₃ H ₁₆ N ₂ O ₈	C ₁₃ H ₁₆ N ₂ O ₈	C ₁₃ H ₁₆ N ₂ O ₇	C ₁₃ H ₁₆ N ₂ O ₇
formula weight	328.28	328.28	312.28	312.28
crystal system	monoclinic	monoclinic	monoclinic	monoclinic
space group	P2 ₁	P2 ₁ /c	C2	P2 ₁ /c
a (Å)	12.4602(1)	12.6137(10)	22.2113(6)	10.7048(3)
b (Å)	8.8777(1)	8.9398(7)	6.0673(2)	6.2392(2)
c (Å)	12.7309(1)	12.5452(8)	11.2292(3)	21.4529(8)
β (deg)	103.0525(1)	103.580(7)	112.595(3)	107.200(3)
V (Å ³)	1371.88(2)	1375.10(18)	1397.12(7)	1368.75(8)
Z	4	4	4	4
D _c (g·cm ⁻³)	1.589	1.586	1.485	1.515
T (K)	100	100	100	100
F(000)	688	688	656	656
crystal size (mm ³)	0.3 × 0.3 × 0.1	0.2 × 0.2 × 0.1	0.4 × 0.2 × 0.2	0.2 × 0.1 × 0.1
μ (mm ⁻¹)	1.154	1.151	1.046	1.068
R _{int}	0.0283	0.0511	0.0453	0.0310
R ₁ [I > 2σ(I)] ^a	0.0349	0.0526	0.0472	0.0383
wR ₂ [all data] ^a	0.0954	0.1332	0.1258	0.1049
reflns collected	24843	5457	19455	5134
Φ _{max} (deg)	71.82	64.99	72.72	69.98
unique reflns	5278	2259	2748	2516
observed reflns	5070	1893	2562	2066
GOF	1.039	1.051	1.050	1.080
Hooft parameter	0.13(8)		0.16(5)	

$$^a R_1 = \frac{\sum ||F_o| - |F_c||}{\sum |F_o|}, wR_2 = \frac{[\sum [w(F_o^2 - F_c^2)^2] / \sum w(F_o^2)^2]^{1/2}}{P}, w = 1/[\sigma^2(F_o)^2 + (aP)^2 + bP], \text{ where } P = [(F_o^2) + 2F_c^2]/3.$$

were isolated by filtration, washed with diethyl ether, and dried under vacuum. Yield: 0.32 g, 96%. Anal. Calcd for C₁₃H₁₆N₂O₈: C, 47.56; H, 4.91; N, 8.53. Found: C, 47.61; H, 4.93; N, 8.51%. IR data (KBr, cm⁻¹) 3377 vs, 3207 s, 2949 m, 2511 m, 1663 s, 1659 s, 1606 m, 1491 m, 1454 m, 1393 m, 1343 w, 1284 s, 1254 m, 1194 m, 1131 w, 1077 w, 939 m, 867 w, 770 w, 705 w, 607 m, 447 w.

(S-ox)(pa), 3. This compound was prepared by a similar procedure to that of **1** except using **pa** instead of **ga**. Yield: 0.28 g, 90%. Anal. Calcd for C₁₃H₁₆N₂O₇: C, 50.00; H, 5.16; N, 8.97. Found: C, 49.60; H, 5.14; N, 9.04%. IR data (KBr, cm⁻¹) 3417 vs, 3198 s, 2942 m, 1668 s, 1638 s, 1609 m, 1493 w, 1453 m, 1398 m, 1343 s, 1255 s, 1255 s, 1076 w, 1040 s, 971 w, 942 m, 870 w, 797 w, 715 m, 618 m, 444 w.

(RS-ox)(pa), 4. This compound was prepared by a similar procedure to that of **2** except using **pa** instead of **ga**. Yield: 0.27 g, 88%. Anal. Calcd for C₁₃H₁₆N₂O₇: C, 50.00; H, 5.16; N, 8.97%. Found: C, 50.00; H, 5.39; N, 8.92. IR data (KBr, cm⁻¹) 3407 vs, 3299 s, 3212 s, 2934 m, 1669 s, 1640 s, 1607 s, 1491 w, 1445 s, 1403 m, 1341 s, 1241 s, 1030 s, 972 w, 943 m, 873 w, 777 w, 715 m, 615 m, 449 w.

Cocrystals 1–4 can also be obtained by solvent-drop grinding of equimolar amounts of oxiracetam and corresponding cofomers with ethanol.

Single Crystal X-ray Diffraction. Single crystal data for 1–4 were collected at 100 K on an Agilent Xcalibur Nova CCD diffractometer with graphite monochromated Cu Kα radiation (λ = 1.54178 Å). Cell refinements and data reduction were applied using the program of

CrysAlis PRO. All the structures were solved using direct methods to yield the positions of all non-hydrogen atoms, which were refined first isotropically and then anisotropically. The hydroxy group of **RS-ox** in **2** is disordered and was treated with half-occupancies of H and O atoms. All the hydrogen atoms were placed in calculated positions with fixed isotropic thermal parameters and included in the structure factor calculations in the final stage of full-matrix least-squares refinement. All calculations were performed using the SHELXTL system of computer programs.¹⁵ The crystallographic data are summarized in Table 1, and the selected H-bond distances and angles are listed in Table S1 (Supporting Information).

Hygroscopic Tests. The hygroscopic tests were performed in a Memert climate chamber at 25 °C, and the relative humidity (RH) conditions were achieved within sealed desiccators containing the saturated salt solutions of K₂CO₃, NaCl, KCl, and K₂SO₄ for 43, 75, 85, and 98% RH values, respectively.^{16–20} Each sample was sieved using standard mesh sieves to provide sample with approximate particle size ranges of 68–150 μm, and was examined by XRPD after the hygroscopic test.

RESULTS AND DISCUSSION

Crystal Structures. Compound **1** crystallizes in P2₁ chiral space group with a Hooft parameter of 0.13(8), indicating the absolute configuration of **S-ox** can be identified. As shown in Figure 1a, the asymmetric unit of **1** contains two **S-ox** and two

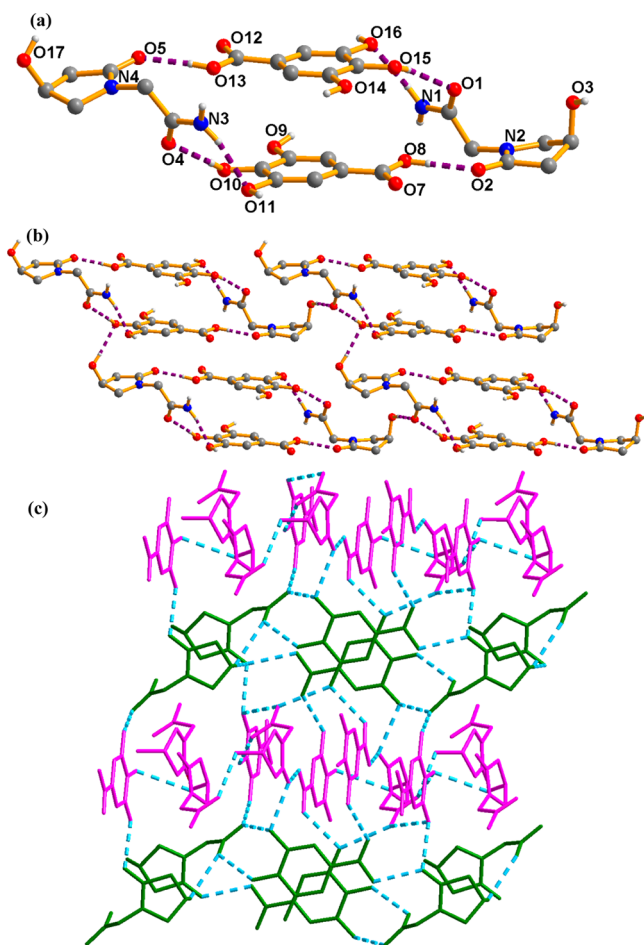


Figure 1. Structures of the (a) tetramer, (b) 2D sheet, and (c) 3D framework in **1** (the purple and green represent two different layers).

ga molecules, and two **ga** molecules link two **S-ox** molecules through four O–H···O and two N–H···O intermolecular hydrogen bonds to form a tetramer, in which the $R_2^2(9)$ synthon constructed by amide and two phenol hydroxy groups has not been reported before. In the tetramer, there are π ··· π stacking interactions between two **ga** molecules, with the centroid···centroid distance of 3.721 Å. The tetramers are further linked by O–H···O intertetramer hydrogen bonds to generate a 2D sheet (Figure 1b). The 2D adjacent sheets are connected by intersheet hydrogen bonds in a crossover packing fashion to form the 3D structure of **1** (Figure 1c).

Compound **2** crystallizes in a monoclinic $P2_1/c$ space group. As shown in Figure 2a, the asymmetric unit of **2** consists of one disordered **ox** (**S-ox** or **R-ox**) molecule and one **ga** molecule. Similar to the structure of **1**, two **ga** molecules in **2** link two disordered **RS-ox** molecules through four O–H···O and two N–H···O intermolecular hydrogen bonds with a $R_2^2(9)$ synthon to form a tetramer (Figure 2a), and there are also existing weak π ··· π stacking interactions between two **ga** molecules, with the centroid···centroid distance of 3.714 Å. Similar to the case of **1**, the tetramers in **2** are also linked by O–H···O intertetramer hydrogen bonds to generate a 2D sheet (Figure 2b), and the adjacent 2D sheets are further connected by O–H···O and N–H···O intersheet hydrogen bonds to form the 3D structure of **2**. It is interesting to note that the density of **2** (1.586 g·cm⁻³) is close to that of **1** (1.589 g·cm⁻³), due to the similar structures of **1** and **2**.

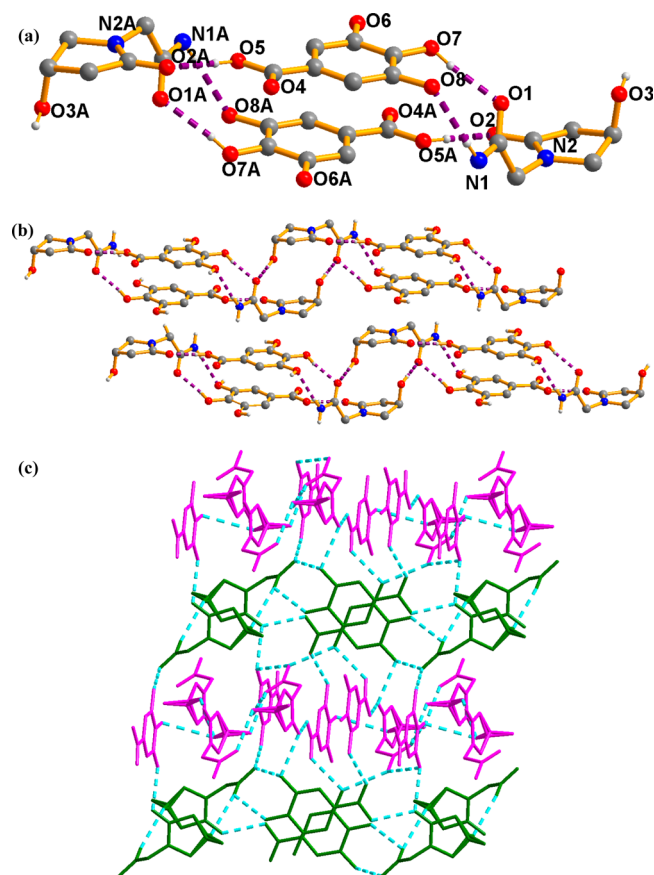


Figure 2. Structures of the (a) tetramer, (b) 2D sheet, and (c) 3D framework in **2** (the purple and green represent two different layers). Symmetry codes: (A) $2 - x, 3 - y, 1 - z$.

Compound **3** crystallizes in the $C2$ chiral space group with a Hooft parameter of 0.16(5), indicating the absolute configuration of **S-ox** can be identified. The asymmetric unit of **3** consists of one **S-ox** and one **pa** molecules. As shown in Figure 3a, the **S-ox** molecules in **3** are linked by intermolecular O–

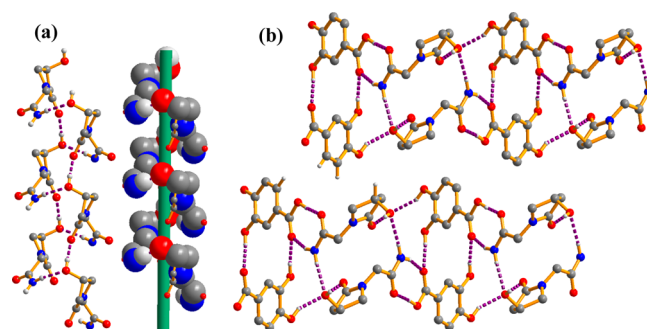


Figure 3. (a) Side view of a 1D hydrogen bonded left-handed helical chain of $(S\text{-ox})_n$ in **3**. (b) The 2D sheets with the same chirality packed along the b -axis.

H···O and N–H···O hydrogen bonds to form a 1D left-handed helical chain of $(S\text{-ox})_n$. The left-handed helical chains are then connected by **pa** molecules through intermolecular O–H···O and N–H···O hydrogen bonds to generate a 2D homochiral sheet (Figure 3b), and all the 2D homochiral sheets are packed along the b axis to form the 3D structure of **3** (Figure 3b).

The asymmetric unit of **4** contains one *S-ox* and one *pa* molecules. It is interesting to note that all *S-ox* molecules in **4** are linked by intermolecular O–H...O and N–H...O hydrogen bonds to form a 1D left-handed helical chain, while all the *R-ox* molecules are linked by similar intermolecular O–H...O and N–H...O hydrogen bonds to form a 1D right-handed helical chain (Figure 4), further confirming the rule we found that

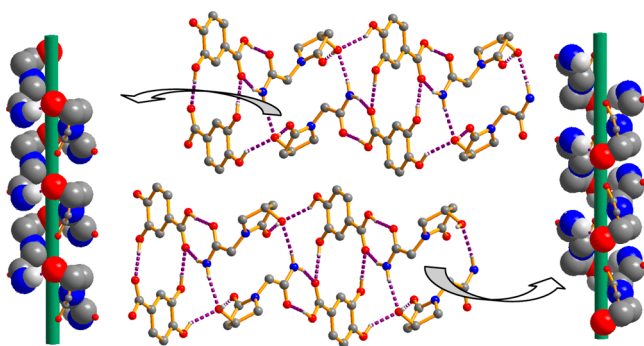


Figure 4. 2D sheets containing the left-handed and right-handed helical chains alternately packed along the *b*-axis in **4**.

there is a correlation between the chirality of building blocks and the helicity of 1D chains.²¹ All the 1D left-handed helical chains are connected by *pa* molecules through intermolecular O–H...O and N–H...O hydrogen bonds to generate a 2D homochiral sheet (Figure 4), while all the 1D right-handed helical chains are connected by *pa* molecules through similar intermolecular O–H...O and N–H...O hydrogen bonds to generate a 2D homochiral sheet with opposite chirality (Figure 4). The above 2D sheets containing the left- and right-handed helical chains are alternately packed along the *b* axis to generate a racemic compound of **4**, which crystallizes in a centrosymmetric space group $P2_1/c$.

X-ray Powder Diffraction and DSC Analyses. XRPD was used to check the phase purity of all the cocrystals. The results indicate that the patterns of the samples prepared by the solvent-drop grinding method fit well with those simulated from the single crystal data (Figure S1), indicating pure phases of cocrystals were obtained by the grinding method. The data of DSC analyses show that the melting point of **1** (183.5 °C) is very close to that of **2** (183.8 °C), while the melting point of **3** (134.6 °C) is much lower than that of **4** (143.4 °C) (Figure S2). In addition, the melting points of cocrystals **1** (183.5 °C) and **2** (183.8 °C) are between those of API ($mp_{S-ox} = 139.0$, $mp_{RS-ox} = 173.7$ °C) and coformer ($mp_{ga} = 250.2$ °C), while the melting points of cocrystals **3** and **4** are lower than those of API and coformer ($mp_{pa} = 200.8$ °C).

Hygroscopic Stability. To check if the hygroscopic stability of *S-ox* can be improved via cocrystals, the hygroscopic stability of *S-ox*, *RS-ox*, and **1–4** was investigated, and the results are shown in Table 2. From Table 2 it can be found that the hygroscopic stability of **1** is much higher than that of *S-ox*, indicating the hygroscopic stability of *S-ox* can indeed be enhanced via cocrystals, and **1** is stable at all relative humidities across all time points. In addition, the hygroscopic stability of **3** and **4** follows a trend of the Wallach's rule, in which the density of racemic **4** (1.515 g·cm⁻³) is higher than that of chiral **3** (1.485 g·cm⁻³) and **4** is more stable than **3**. However, **1** and **2** do not follow the Wallach's rule, as the density of racemic **2** (1.586 g·cm⁻³) is close to that of chiral **1** (1.589 g·cm⁻³), and **1** and **2** show similar hygroscopic stability under our hygroscopic

Table 2. Hygroscopic Test for APIs and Cocrystals at 25 °C^a

sample	RH	1 day	3 days	7 days	14 days	28 days	8 weeks
<i>S-ox</i>	43%	✓	✓	✓	✓	✓	✓
	75%	✓	✓	✓	✓	✓	✓
	87%	✓	×	×	×	×	×
	98%	×	×	×	×	×	×
<i>RS-ox</i>	43%	✓	✓	✓	✓	✓	✓
	75%	✓	✓	✓	✓	✓	✓
	87%	✓	✓	✓	✓	✓	✓
	98%	✓	×	×	×	×	×
1	43%	✓	✓	✓	✓	✓	✓
	75%	✓	✓	✓	✓	✓	✓
	87%	✓	✓	✓	✓	✓	✓
	98%	✓	✓	✓	✓	✓	✓
2	43%	✓	✓	✓	✓	✓	✓
	75%	✓	✓	✓	✓	✓	✓
	87%	✓	✓	✓	✓	✓	✓
	98%	✓	✓	✓	✓	✓	✓
3	43%	✓	✓	✓	✓	✓	✓
	75%	✓	✓	✓	✓	✓	✓
	87%	✓	✓	×	×	×	×
	98%	✓	×	×	×	×	×
4	43%	✓	✓	✓	✓	✓	✓
	75%	✓	✓	✓	✓	✓	✓
	87%	✓	✓	✓	✓	✓	✓
	98%	✓	✓	✓	×	×	×

^aThe symbol ✓ means that the crystalline compound was stable at that condition and time point, and the symbol × means that the compound deliquesced to a liquid at that condition and time point.

conditions. We also performed the XRPD measurements for samples **1–4** after the hygroscopic stability test for 8 weeks (see Table 2), and we found that the phases for all the samples without deliquescing remain unchanged, indicating samples **1–4** are stable and did not convert to drug and/or to conformer before deliquescing (deliquescing means the sample becomes a liquid). The overall hygroscopic stability trend is summarized as **1** ≈ **2** > **4** > *RS-ox* > **3** > *S-ox*. Gallic acid (*ga*) and 3,4-dihydroxybenzoic acid (*pa*) can absorb moisture to form hydrate at 87% and 98% RH, respectively. Obviously, the lower hygroscopic stability of **3** and **4** is not caused by the hygroscopicity of coformers. The highest stability of **1** and **2** mainly attributes to the introduction of additional hydrogen bonding stabilization, as *ga* contains three hydroxyl groups, while *pa* only contains two hydroxyl groups: one additional hydroxyl group in *ga* can form more hydrogen bonds with *S-ox* and *RS-ox* in **1** and **2** to generate 3D hydrogen bonded frameworks, while **3** and **4** only form 2D sheets; thus, the hygroscopic stability of **1** and **2** is higher than that of **3** and **4**.

CONCLUSIONS

Four cocrystals of **1–4** were prepared by the methods of solution evaporation and solvent-drop grinding, in which **1** and **2** form 3D hydrogen bonded frameworks with a new R₂²(9) synthon, while **3** and **4** exhibit 2D homochiral and racemic sheets containing 1D helical chains. The results of hygroscopic stability measurements indicate that the hygroscopic stability of *S-ox* has been much enhanced after the formation of cocrystals **1**. In addition, the hygroscopic stability of **3** and **4** follows a trend of Wallach's rule, while **1** and **2** do not follow a trend of such rule. Cocrystals **1** and **2** are stable at all relative humidities

and for all time points we tested, due to their more extended hydrogen bonded frameworks.

■ ASSOCIATED CONTENT

📄 Supporting Information

H-bond distances and angles, the XPRD patterns, DSC curves, and CIF data for 1–4. This material is available free of charge via the Internet at <http://pubs.acs.org>.

■ AUTHOR INFORMATION

Corresponding Author

*Fax: +86-20-84112921. E-mail: chenjm37@mail.sysu.edu.cn; lutongbu@mail.sysu.edu.cn.

Notes

The authors declare no competing financial interest.

■ ACKNOWLEDGMENTS

This work was financially supported by 973 Program of China (2012CB821705) and NSFC (Grant Nos. 91127002, 21101173, 21121061, and 20831005).

■ REFERENCES

- (1) Caner, H.; Groner, E.; Levy, L.; Agranat, I. *Drug Discovery Today* **2004**, *9* (3), 105–110.
- (2) Food and Drug Administration. *Fed. Reg.* **1992**, *22*, 249.
- (3) Chen, Y.; Rong, Z.; Li, K.; Ping, Y.; Yu, Y. *CN Patent* 101575309, 2009.
- (4) Bandoli, G.; Grassi, A.; Nicolini, M. *Chem. Pharm. Bull.* **1985**, *33*, 4395–4401.
- (5) Rong, Z.; Jin, L.; Feng, H.; Li, F.; Li, B.; You, C.; Pang, Q.; Xu, N.; Ye, L. *CN Patent* 102204904, 2010.
- (6) Brock, C. P.; Schweizer, W. B.; Dunitz, J. D. *J. Am. Chem. Soc.* **1991**, *113*, 9811–9820.
- (7) Friscic, T.; Fabian, L.; Burley, J. C.; Reid, D. G.; Duer, M. J.; Jones, W. *Chem. Commun.* **2008**, 1644–1646.
- (8) Bethune, S. J.; Schultheiss, N.; Henck, J. *Cryst. Growth Des.* **2011**, *11*, 2817–2823.
- (9) Clarke, H. D.; Arora, K. K.; Bass, H.; Kavuru, P.; Ong, T. T.; Pujari, T.; Wojtas, L.; Zaworotko, M. J. *Cryst. Growth Des.* **2010**, *10*, 2152–2167.
- (10) Cherukuvada, S.; Babu, N. J.; Nangia, A. *J. Pharm. Sci.* **2011**, *100*, 3233–3244.
- (11) Schultheiss, N.; Newman, A. *Cryst. Growth Des.* **2009**, *9*, 2950–2967.
- (12) Shan, N.; Zaworotko, M. J. *Drug Discovery Today* **2008**, *13*, 440–446.
- (13) Landenberger, K. B.; Matzger, A. J. *Cryst. Growth Des.* **2010**, *10*, 5341–5347.
- (14) Masibo, M.; He, Q. Blackwell Publishing Inc.: 2008; Vol. 7, pp 309–319.
- (15) Sheldrick, G. M. *SHELXTL-97, Program for Crystal Structure Solution and Refinement*; University of Göttingen: Göttingen, Germany, 1997.
- (16) Trask, A. V.; Motherwell, W. D. S.; Jones, W. *Cryst. Growth Des.* **2005**, *5*, 1013–1021.
- (17) Trask, A. V.; Motherwell, W. D.; Jones, W. *Int. J. Pharm.* **2006**, *320*, 114–123.
- (18) Good, D.; Miranda, C.; Rodríguez-Hornedo, N. *CrystEngComm.* **2011**, *13*, 1181–1189.
- (19) Reddy, L. S.; Bethune, S. J.; Kampf, J. W.; Rodríguez-Hornedo, N. *Cryst. Growth Des.* **2009**, *9*, 378–385.
- (20) Jayasankar, A.; Roy, L.; Rodríguez-Hornedo, N. *J. Pharm. Sci.* **2010**, *99*, 3977–3985.
- (21) Zheng, X. D.; Lu, T. B. *CrystEngComm* **2010**, *12*, 324–336.